Journal of Materials Chemistry B

Accepted Manuscript

ROYAL SOCIETY OF CHEMISTRY

www.rsc.org/materialsB

Layered tungsten disulfide/acetylene black composites based DNA biosensing platform coupled with hybridization chain reaction for signal amplification

Hong-Lei Shuai, Ke-Jing Huang,* Ying-Xu Chen

College of Chemistry and Chemical Engineering, Xinyang Normal University, Xinyang 464000, China

*Corresponding author. Tel.: +86-376-6390611

E-mail address: kejinghuang11@163.com (K.J. Huang)

ABSTRACT: 2-Dimensional tungsten disulfide-acetylene black (WS_2-AB) composite is synthesized by a simple hydrothermal method to achieve excellent electrochemical properties for applications as DNA biosensor. The biosensor is fabricated based on the Au nanoparticles (AuNPs) and WS_2-AB composites modified electrode, which subsequently is used to couple with capture probe by Au-S bond, then modified with target DNA, auxiliary DNA and bio-H1-bio-H2 (H1-H2) to perform hybridization chain reaction for signal amplification. Herein, two DNA hairpins H1 and H2 are opened by the recognition probe. The nicked double helices from hybridization chain reaction are used to immobilize horseradish peroxidase enzymes via biotin-avidin reaction, which produces signal-amplification detection of target DNA through the catalytic reaction of hydrogenperoxide + hydroquinone system. Under optimum conditions, the as-prepared biosensor shows a good linear relationship between the current value and logarithm of the target DNA concentration ranging from 0.001 pM to 100 pM and a detection limit as low as 0.12 fM. Moreover, the fabricated biosensor exhibits good selectivity to differentiate one-base mismatched DNA sequence. This work will open a pathway for ultrasensitive detection of other biorecognition events and gene-related diseases based on layered WS_2-AB and hybridization chain reaction.

1. Introduction

Ultrasensitive and highly selective detection of nucleic acids has attracted considerable interest and some assays have been developed for this purpose, such as fluorescence and electrochemical methods.[1,2] For example, Peng et al. have proposed a series of fluorescent methods for ultrasensitive detection of nucleic acids.[3-8] Electrochemical DNA sensors have gained particular attractive due to their superior features of low cost, simplicity, portability and rapid response.[9] Since the DNA sequences of interest are present in very small amounts, it is essential to develop exponential amplification techniques that enable to detect trace levels of a specific sequence.[10] Therefore, the development of signal amplification strategies to fabricate ultrasensitive DNA biosensor has recently received particular interest.[11,12] One of signal amplification strategies is post amplification strategy toward the signal produced by hybridization event,[13] and it can improve on the sensitivity in the electrochemical detection of DNA by metal nanoparticles,[14] enzyme-aided reactions,[15] DNA biobarcode[16] and redox indicators[17] as the signal amplifying labels. As an advanced DNA assembly technology, hybridization chain reaction (HCR) has recently developed as an attractive tool for signal amplification toward DNA detection due to its significant advantages such as simple, cost-effective, sensitive and selective.[18] Target acts as an initiator to trigger the hybridization reaction during the course of HCR, which leads to the formation of long-range of DNA sequence in a long nicked duplex DNA. The initiator triggered reaction generates a low pseudo-positive result, leading to a high signal to noise ratio. Furthermore, every target can trigger a HCR

event to form a long-range DNA sequence, which shows great potential in the sensitive detection of DNA. It is worth mentioning that the products of HCR are highly ordered DNA double helices, which can precisely control density to combine signaling molecules. Till now, HCR has extensively been applied for signal-amplification detection of various analytes.[18,19]

Acetylene black (AB), a special kind of carbon black with porous structure, has attracted a great amount of attention because of extraordinary properties, such as high accumulation efficiency, excellent electric conductivity, large surface area, high catalytic activity and strong adsorptive ability.[20,21] It has been used for the fabrication of electrochemical sensor to improve the detection sensitivity and the response signal.[22,23]

Two-dimensional (2D) layered compounds have attracted immense interest in the field of electrochemistry in the past decade, such as WS_2, MoS_2, SnS_2, CoS_2 and VS_2 etc. They have been successfully established as a new paradigm in the chemistry and biosensing due to their large surface area and fast heterogeneous electron transfer.[24-26] From the structural point of view, WS_2 is a typical member of 2D layered compounds. It is composed of the metal W layer sandwiched between two sulfur layers and stacked together by weak Van der Waals interactions.[27] The layered structure of WS_2 is expected to act as an excellent functional material due to the 2D electron correlations among W atoms would aid in enhancing planar electric transportation properties. In fact, WS_2 has attracted considerable attention due to its extensive applications as electrocatalysis, lubricants, lithium battery, supercapacitors, and so

on.[28-30] Nevertheless, few attentions have been put into its application as an electrode material for electrochemical sensing because the electronic conductivity of WS_2 is still relative low as similar with the most transition metal oxides. To overcome this problem, hybrid materials that incorporation of WS_2 with good electronic conductive materials seem imperative.

In this work, layered 2D tungsten disulfide/acetylene black (WS_2-AB) composite was synthesized by a simple hydrothermal method. An ultrasensitive electrochemical DNA biosensor was fabricated based on the Au nanoparticles (AuNPs) and WS_2-AB composites modified glassy carbon electrode (GCE), which possessed low background current, good conductivity and large electroactive surface area. The probe ssDNA was linked to the modified electrode via Au-S bond. Afterward, auxiliary DNA was immobilized on the modified electrode. The auxiliary DNA had a sequence complementarity to target DNA and it may expedite target DNA to HCR with H1-H2 on the electrode surface and enhanced the selectivity of the sensor. The two DNA hairpins H1-H2 were opened by the recognition probe. The nicked double helices from hybridization chain reaction were used to immobilize horseradish peroxidase enzymes via biotin-avidin, which produced signal-amplification detection of target DNA through the catalytic reaction of hydrogenperoxide + hydroquinone system. As 2D layered nanostructure, the as-prepared WS_2-AB displayed large effective surface area. This allowed more biomolecules (capture DNA) to be immobilized at the electrode surface, which reduced the distance for electron transfer and ion diffusion paths between the capture DNA and nanomaterials. As a result, the charge transfer to

the electrodes became easier. In addition, the strong interactions between the capture DNA and electrode surface enhanced the surface density of the immobilized analytes, which therefore led to a low detection limit. Under optimal experimental conditions, the proposed DNA biosensor showed a sub-femtomolar detection limit for the target DNA with a wide linear range and good selectivity.

2. Experimental

2.1. Reagents and apparatus

$K_3Fe(CN)_6$, $K_4Fe(CN)_6$ and chloroauric acid ($HAuCl_4 \cdot 4H_2O$) were purchased from Sigma-Aldrich (St. Louis, MO). The other chemicals were of analytical grade and used without further purification. All aqueous solutions were prepared using ultra-pure water (≥18.2 MΩ, Milli-Q, Millipore). All DNA sequences were synthesized by Shanghai Sangon Biological Engineering Technological Co. Ltd. (China). The sequences of synthesized DNA are shown in Table 1 and the buffers used in this work are shown in Table 2.

Table 1 DNA sequences employed in this work.

Oligonucleotides	Sequences (5'- 3')
Capture probe	5'-TGCAGTTTCCGTCCGTAGTTTTT-SH-3'
Target DNA	5'-CTACGGACGGAAACTGCACCTGTATTCCCATACCCATCAT-3'
One-based mismatch DNA Three-based	5'-CTACGGACGGAAACTGCAACTGTATTCCCATACCCATCAT-3'
Three-based mismatch DNA	5'-CTACGGACGCAAACTGCAACTGTATTCTCATACCCATCAT-3'
Noncomplementary	5'-CTGCTTCCAAACCTTTAACATAGCCGCAAGCGTTAGCTGC-3
Auxiliary DNA	5'-AGTCTAGGATTCGGCGTGGGTTAAATGATGGGTATGGGAATACAGG-3'
Bio-H1	5'-biotin-TTAACCCACGCCGAATCCTAGACTCAAAGTAGTCTAGGATTCGGCGTG-3'
Bio-H2	5'-biotin-AGTCTAGGATTCGGCGTGGGTTAACACGCCGAATCCTAGACTACTTTG-3'

Table 2 Buffers used in this work.

Buffer	Solute and pH	Application
1	PBS1 (10 mM PBS, 3 M NaCl and 2.7 mM KCl, pH 7.4)	Capture DNA
2	PBS2 (10 mM PBS, 150 mM NaCl, 2.7 mM KCl and 10 mM $MgCl_2$, pH 7.4)	Target DNA, Auxiliary DNA, Mismatch DNA
3	PBS3 (50 mM PBS and 1 M NaCl, pH 7.4)	Bio-H1, Bio-H2

All electrochemical measurements were performed on an EC550 electrochemical workstation (Wuhan, Gaoss Union, China) except electrochemical impedance

spectroscopy (EIS) measurements were carried out on a RST5200F electrochemical workstation (Zhengzhou Shi Rui Si Instrument China) with a conventional three-electrode system composed of a platinum wire as an auxiliary electrode, a saturated calomel electrode (SCE) as a reference electrode and a 3-mm diameter GCE as a working electrode. Nanostructures were characterized by a JEM 2100 transmission electron microscope (TEM, JEOL, Tokyo, Japan) and a Hitachi S-4800 scanning electron microscope (SEM, Tokyo, Japan). X-ray diffraction (XRD) pattern was operated on a model D/max-rA diffractometer (Rigaku, Japan). Raman spectra were recorded at ambient temperature on a Renishaw Raman system model 1000 spectrometer (Gloucestershire, UK). Fourier transform infrared spectroscopy (FT-IR) was measured on a Bruker-Tensor 27 IR spectrophotometer (Ettlingen, Germany).

2.2. Synthesis of WS_2, AB and WS_2-AB nanocomposites

WS_2 nanosheets were prepared according to a previous protocol.[31] Commercial WS_2 powder was first ground by ball grinding mill for 3 h. Subsequently, the WS_2 powder (40 mg) was added in 40 mL sulfuric acid and refluxed for 24 h at 90 °C. The as-prepared products were collected by centrifugation and washed with water for several times to remove the residual H_2SO_4. Finally, the WS_2 nanosheets were dried in a vacuum oven at 70 °C for 24 h.

AB was firstly treated by concentrated nitric acid. In short, 1.0 g AB was added in 200 mL concentrated nitric acid and then refluxed at 140 °C for 2.0 h. After cooling, the black product was washed thoroughly with water until the pH was close to 7, and

then dried at 80 ℃ for 24 h. WS_2-ABcomposites were synthesized by a simple hydrothermal method. Five WS_2-AB composites with mass ratios of WS_2 to AB of 0.5:1, 1:1, 1.5:1, 2:1 and 3:1 were synthesized as follows: firstly, 1 mg WS_2 was ultrasonically dispersed in 40 mL deionized water, and AB with different mass (0.5, 1.0, 1.5, 2.0 and 3.0 mg) was then added and ultrasonically dispersed for 30 min. After that, the mixture was diluted with water to 80 mL and transferred to a 100 mL Teflon-lined stainless steel autoclave and heated at 180 ℃ for 48 h. After cooling to room temperature naturally, the WS_2-AB nanocomposites were collected by centrifugation, washed with water for several times, and finally dried in vacuum oven at 80 ℃ for 24 h.

2.3. Preparation of DNA biosensor and electrochemical measurements

For electrode preparation, 1.0 mg WS_2-AB nanocomposites were dispersed in 1 mL water with uitrasonication for 20 min to get homogenous suspension (1 mg mL^{-1}). The bare GCE was polished sequentially with 0.3 and 0.05 μm alumina slurries, washed ultrasonically with water and ethanol and then dried with nitrogen gas. The WS_2-AB composites modified electrode was prepared by applied 6 μL suspension onto the cleaned GCE and dried in the air. For assembling the probe DNA, the AuNPs was electrodeposited on WS_2-AB/GCE from a PBS (pH 7.0) solution containing 0.1% $HAuCl_4$ at a constant potential of −0.2 V for 60 s. After that, 8 μL of 0.5 μM probe DNA solution was dropped onto the AuNPs/WS_2-AB/GCE and allowed to react overnight. After thoroughly washed with PBS to remove the unbound probe DNA, 8

183 μL of 1% BSA was dropped on the probe DNA/AuNPs/WS_2-AB/GCE surface for 30
184 min to eliminate nonspecific adsorption. After the electrode was rinsed with buffer
185 solution, 8 μL target DNA was applied on the BSA/capture
186 probe/AuNPs/WS_2-AB/GCE and incubated for 90 min at 37 ℃. Afterward, the
187 auxiliary DNA was added on the electrode and incubated at 37 ℃ for 40 min. H1 and
188 H2 samples were heated to 95 ℃ for 5 min and then allowed to cool to room
189 temperature for 2 h. After that, the sample was diluted with PBS3 to the final
190 concentration of 0.5 μM, and then 8 μL mixture was coated on the electrode and
191 incubated at room temperature for 50 min for the HCR. 6 μL avidin-HRP (0.5 μM
192 mL^{-1}) was then dropped on the modified electrode and incubated for 35 min. Finally,
193 the resulting Avidin-HRP/auxiliary DNA/target DNA/BSA/capture
194 probe/AuNPs/WS_2-AB/GCE was rinsed with distilled water and used for
195 electrochemical measurements.

196 For DNA sensing, cyclic voltammetry (CV) was carried out in 0.1 M PBS (pH
197 7.0) containing 1.0 mmol L^{-1} $[Fe(CN)_6]^{3-/4-}$ and 0.1 mol L^{-1} KCl solution between a
198 potential window of −0.2 V and 0.6 V with a scan rate of 100 mVs^{-1}. EIS
199 measurements were performed in 0.1 M PBS (pH 7.0) containing 5.0 mmol L^{-1}
200 $[Fe(CN)_6]^{3-/4-}$ and 0.1 mol L^{-1} KCl solution, with the AC voltage amplitude of 5 mV,
201 the voltage frequencies from 100 KHz to 0.1 Hz and the applied potential of 0.2 V.
202 The DPV measurements were conducted in the potential region from −0.4 V to 0.2 V
203 (vs. SCE) in 0.1 M PBS (pH 7.0) containing 2 mM HQ and 1.8 mM H_2O using a
204 pulse amplitude of 50 mV, pulse width of 50 ms and pulse period of 0.2 s.

205

206 3. Results and discussion

207 3.1 Design principle of the DNA biosensor

208 The principle of DNA biosensor fabrication is illustrated in Scheme 1. First, the 2D
209 WS_2-AB composites are prepared and used as supporting substrate of the biosensor
210 due to their large specific surface area and good electro-conductivity. After AuNPs are
211 deposited on the WS_2-AB modified GCE, the designed thiolated probe DNA sequence
212 which is complementary with target DNA is immobilized on the
213 AuNPs/WS_2-AB/GCE to form an upright probe through the Au-S bond. In the
214 presence of target DNA, the probes DNA can hybridize with target DNA on the
215 electrode. After that, auxiliary DNA hybridizes with target DNA and the two species
216 of DNA hairpins bio-H1 and bio-H2 are opened by the recognition probe, and
217 hybridizes one by one. In the present design, two complementary hairpins Bio-H1 and
218 Bio-H2 are stable and would not open or hybridize each other at room temperature.
219 Since the two hairpins are modified with biotin, lots of biotin can be introduced onto
220 the electrode by the hybridization between auxiliary DNA and H1-H2. When the
221 avidin-HRP is added, it can result in a strongly current response by the catalysis of
222 HRP to the mixture of H_2O_2 and HQ, and thus leads to the signal amplification.

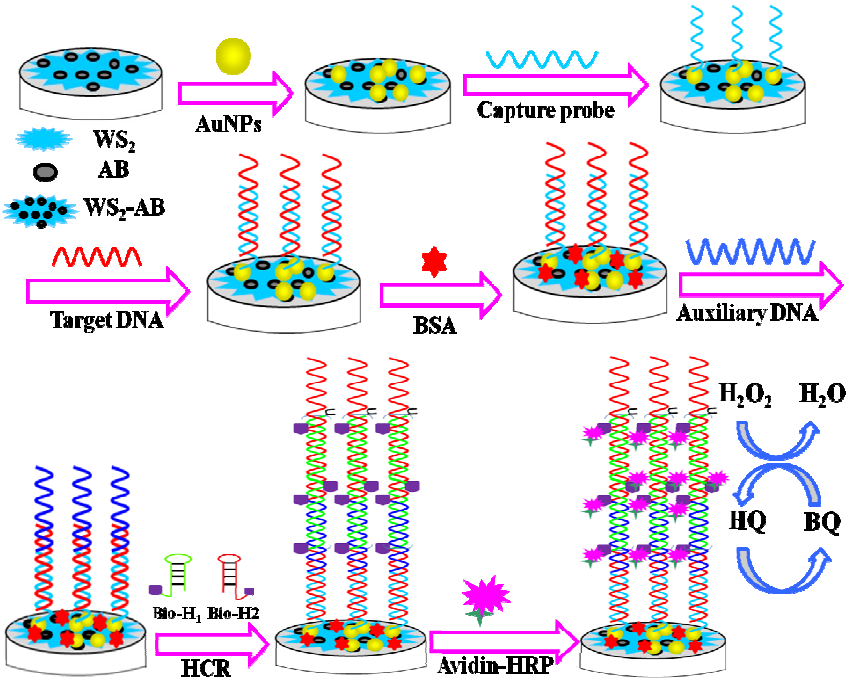

Scheme 1. Schematic illustration of working principle of DNA detection based on hybridization chain reaction.

3.2. Characterization

The morphologies of the as-prepared samples were characterized by SEM and TEM. Fig. 1 A–C displays the SEM images of different samples. The SEM image in Figure 1 A reveals the layered WS_2 sheets, illustrating the flake-like shape of WS_2. The SEM image of AB is shown in Figure 1 B. Many nanocarbon oblate spheroids with diameters ranging from 20 to 50 nm are observed. The SEM image of WS_2-AB composites are showed in Figure 1 C. It exhibits AB cumulates and distributes well on the 2D WS_2 skeleton, evidencing the well-behaved assembly process. This layered architecture is helpful to increase specific surface area of the WS_2-AB composite, which is benefit to load more cDNA and therefore lead to a low detection limit of analytes.

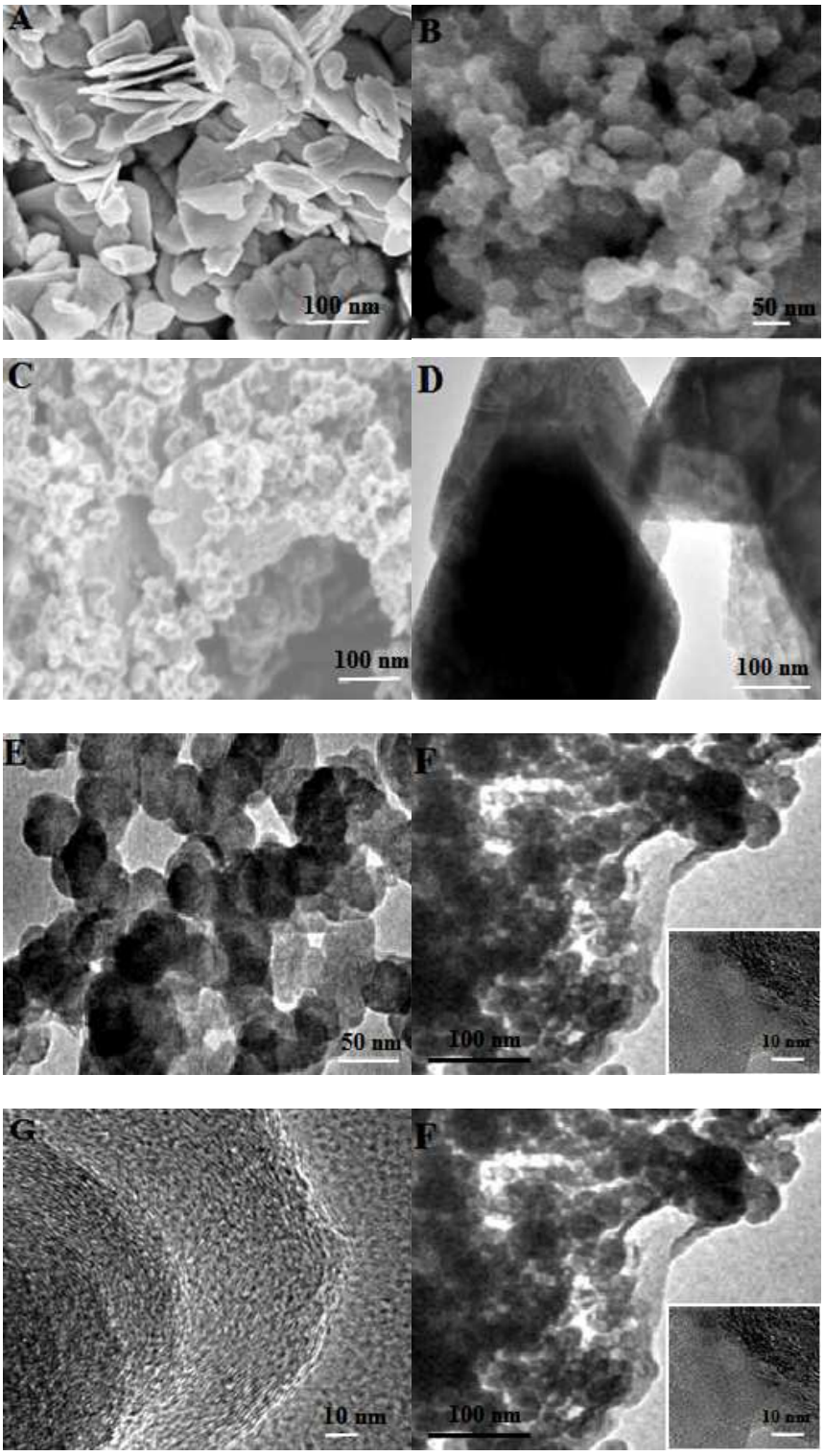

Figure 1. SEM images of WS_2 (A), AB (B) and WS_2-AB composites (C); TEM images of WS_2 (D), AB (E) and WS_2-AB composites (F); HRTEM images of WS_2-AB composites (G, H).

In order to reveal the fine microstructure, the synthesized WS_2, AB and WS_2-AB composites were characterized by TEM and HRTEM. Figure 1D shows the flake-like shape of WS_2. As shown in Figure 1E, the AB exhibits the typical oblate spheroid structure. From Figure 1F, it can be clearly seen that AB is cumulated and distributed on the layered WS_2. In the illustrations, the HRTEM image of the WS_2-AB clearly shows WS_2 has linear lattice fringe and AB shows the typical lattice fringe of carbon material which is similar to fingerprints, indicating AB distributed well on the WS_2 surface. The HRTEM images of the WS_2-AB in Figure 1G and H show the layered WS_2 has defects or disorder structure.

Good dispersibility of the composites plays an important role in the construction of stable electrochemical sensor. Herein, WS_2, AB and WS_2-AB composites are dispersed in water by vigorous shaking. Figure 2A shows that AB and WS_2-AB composites display the homogenous black solution and WS_2 nanosheets produce silvery grey solution. The WS_2 and AB subside to the bottom after left to stand for three days while the WS_2-AB composites still disperse well in the water (Figure 2B), indicating good dispersibility of WS_2-AB composite.

Figure 2C records the XRD patterns of WS_2, AB and WS_2-AB composites. It can be seen that diffraction of WS_2 alone shows the typical peaks at 14.3°, 28.9°, 32.7°, 33.5°, 39.8°, 43.9° and 49.6°, which correspond to (002), (004), (100), (101), (103), (006) and (105) planes of WS_2 (JCPDS No. 37-1492), respectively. Two broad diffraction peaks center at about 25.7° and 42.5°corresponding to AB are observed. The main diffraction peaks of WS_2 display very weak, indicating AB densely covered

on the surface of WS_2 nanosheets. For WS_2–AB composites, the presence of diffraction peaks centered at 14.3°, 25.7°, 28.9°, 32.7°, 33.5°, 39.8°, 43.6° and 49.6° suggests a few-layered structure for WS_2 and AB.

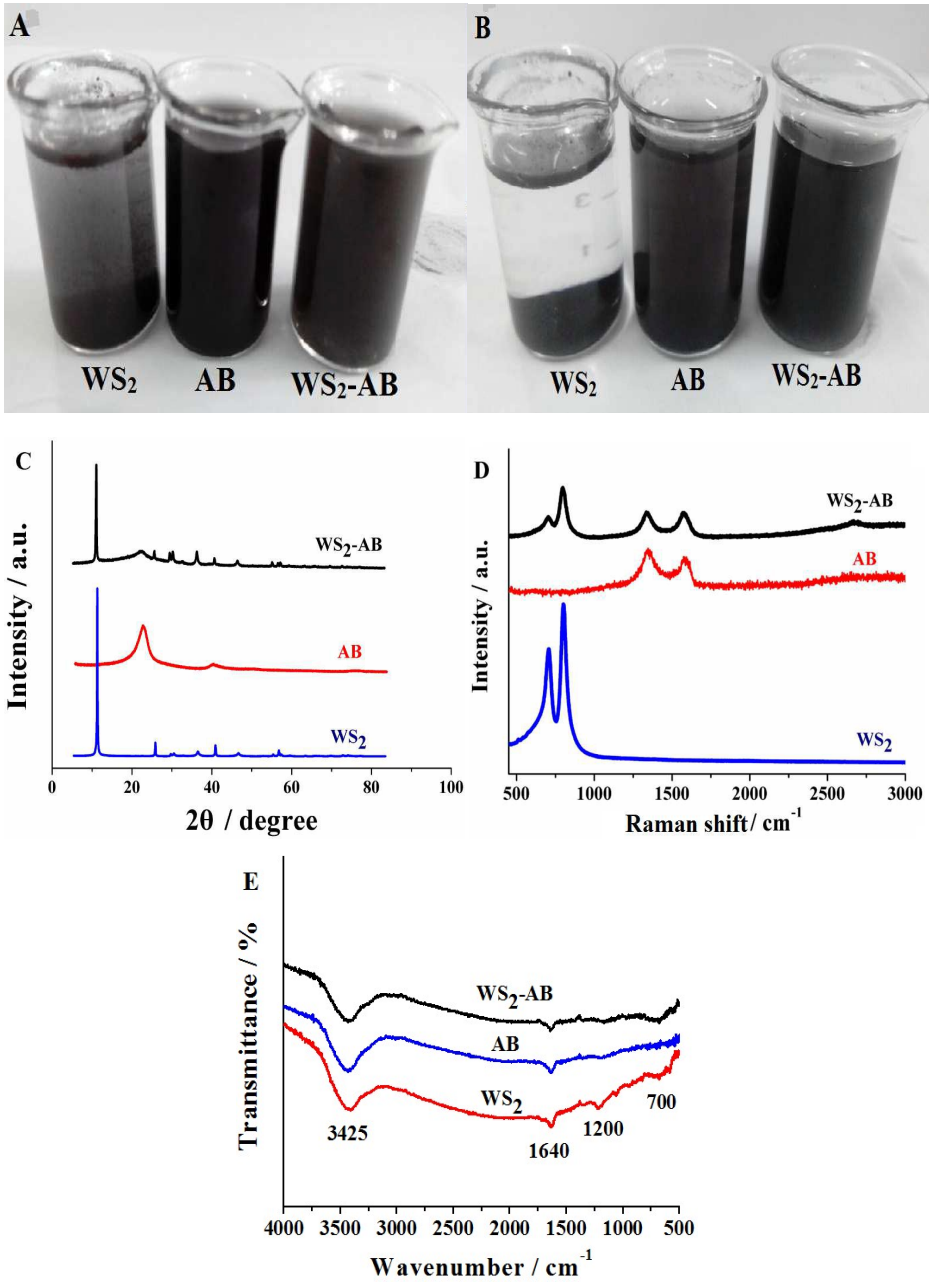

Figure 2. (A, B) The photograph of WS_2, AB and WS_2-AB composites dispersed solution: (A) vigorous shaking for 30 min; (B) left to stand for three days; (C) XRD patterns of WS_2, AB and WS_2-AB composites; (D) Raman spectra of WS_2, AB and WS_2-AB composites; (E) FT-IR spectra of WS_2, AB and WS_2-AB composites.

Further insights of the structural and electronic properties of products were obtained from Raman spectrum (Figure 2D). The Raman spectrum of AB exhibits the *D* band at 1350 cm^{-1} that arises from sp^3-hybridized carbon and the *G* bands at 1590 cm^{-1} which represents the E_{2g} zone center mode of the crystalline graphite. The characteristic bands of WS_2 observed at 709 cm^{-1} and 800 cm^{-1} correspond to the E_{2g} and A_{1g} modes, respectively. The WS_2–AB composites show the peaks at 1348 cm^{-1} and 1589 cm^{-1}, which are assigned to the *D* and *G* peaks of the AB and 709 cm^{-1} and 800 cm^{-1} corresponds to the WoS_2, respectively, thus confirming the presence of the AB and WS_2 in the composite and complete correspondence with the findings from the XRD diffraction studies.

FT-IR spectra of different samples were compared between 4000 and 500 cm^{-1}. As shown in Figure 2E, no significant difference is observed between the spectra with respect to the wave number of major bands for the AB and WS_2–AB composites. The bond at 3425 cm^{-1} is mainly assigned to stretching vibrations of the O–H bonds. The difference on the intensity of the OH vibration indicates that the free hydroxy groups increase after WS_2 combined with AB. This is helpful to increase the dispersibility of WS_2–AB composite in water, and this characteristic helps to develop stable electrochemical sensor. The weak peak at about 700 cm^{-1} at WS_2-AB and WS_2 spectra is assigned to W-S vibration.

3.3. Electrochemical characterization

As shown in Figure 3A, the CV at the bare GCE electrode shows the lowest reduction

peak current of 12 μA (curve a). Five WS_2-AB composites with mass ratios of WS_2 to AB (0.5:1, 1:1, 1.5:1, 2:1 and 3:1) are applied on GCE and five reduction peak currents of 28.1 μA (curve e), 31.3 μA (curve f), 23.5 μA (curve d), 18.7 μA (curve c) and 15.3 μA (curve b) are obtained, respectively. The electrode modified of WS_2-AB composites with mass ratios of WS_2 to AB of 1:1 shows the highest peak current. So it was used in the further experiments.

Figure 3B shows the lowest reduction peak current of 12 μA at the bare GCE electrode (curve a). The presence of AB on the GCE yields a reduction peak current of 19.4 μA (curve b) due to the reduced electron transfer resistance. When WS_2-AB composites are immobilized on the electrode, a corresponding peak current of 31.6 μA (curve c) is observed due to the large specific surface area and the good conductor of the composites. The highest reduction peak current (33.4 μA) obtained at the AuNPs/WS_2-AB/GCE (curve d) indicates the synchronous introduction of WS_2-AB and AuNPs on the electrode effectively enhances the peak currents, which is due to the effective integration of individual advantages of WS_2–AB and AuNPs (such as large surface area and excellent electronic conductivity). In addition, the reduction peak current of the capture probe/WS_2-AB/GCE (curve e) obviously decreases due to the electrostatic repellence between negatively charged phosphate of DNA and negative charged $[Fe(CN)_6]^{3-/4-}$. The peak current of BSA/capture probe/AuNPs/WS_2-AB/GCE (curve e) further decreases because BSA is a biological macromolecule, which hinders the electron exchange on the surface of the electrode. The peak current of the target DNA/BSA/capture probe/AuNPs/WS_2-AB/GCE (curve

f), auxiliary DNA/target DNA/BSA/capture probe/AuNPs/WS_2-AB/GCE (curve h) and HCR/auxiliary DNA/target DNA/BSA/capture probe/AuNPs/WS_2-AB/GCE (curve i) gradually decreases due to specific binding among DNA. More and more DNA sequences are fixed on the electrode surface make the DNA chain extend and the electron transfer become more difficult.

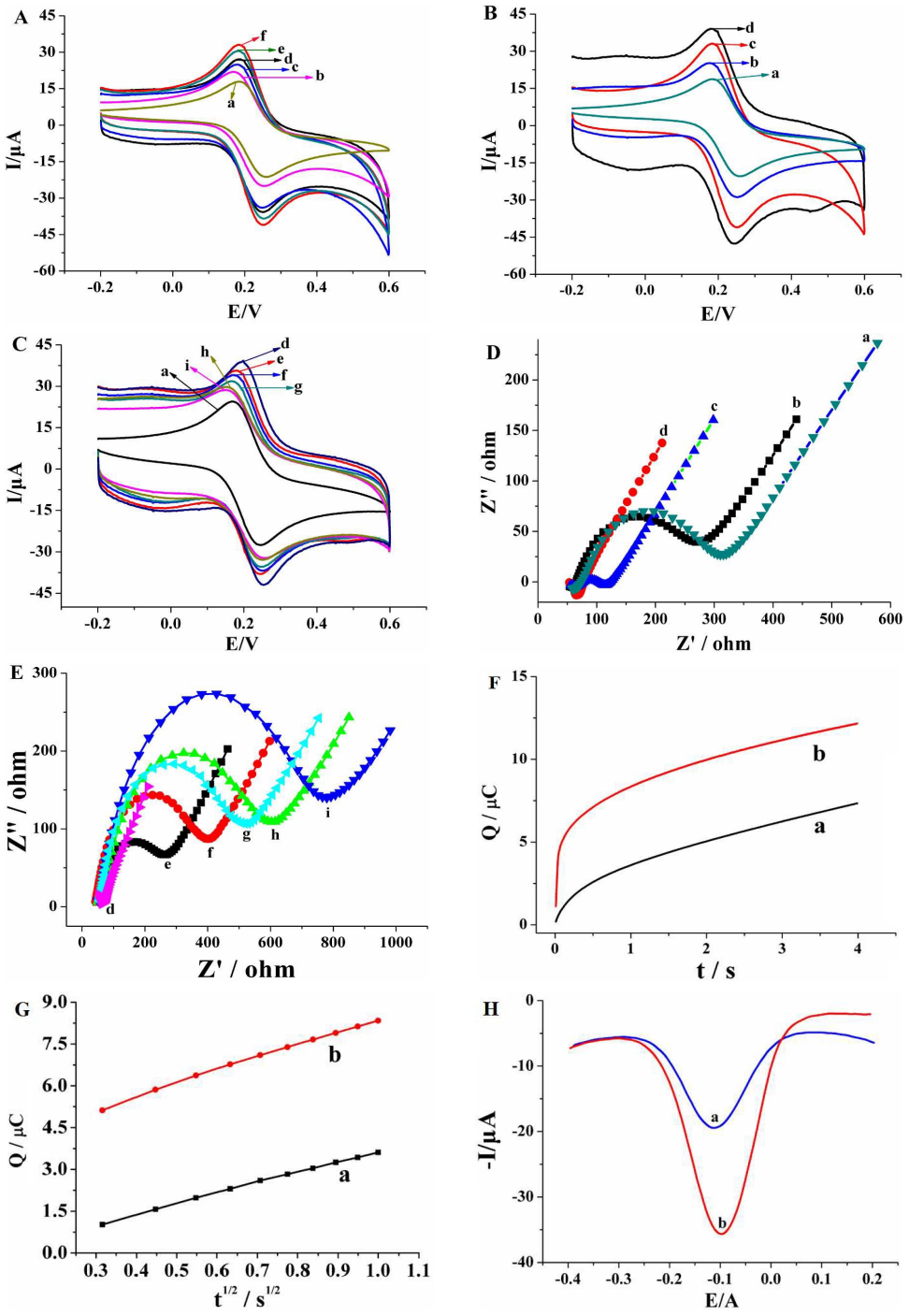

Figure 3. (A) CVs of GCE (a) and different mass ratios of WS_2 and AB in composites: 3:1 (b), 2:1 (c), 1.5:1 (d), 0.5:1 (e), 1:1 (f); CVs (B, C) and EIS (D, E) of bare GCE (a), AB/GCE (b), WS_2-AB/GCE (c), AuNPs/WS_2-AB/GCE (d), capture probe/AuNPs/WS_2-AB/GCE (e), BSA/capture probe/AuNPs/WS_2-AB/GCE (f), target/capture probe/BSA/AuNPs/WS_2-AB/GCE (g), auxiliary/target/capture probe/BSA/AuNPs/WS_2-AB/GCE (h), HCR/auxiliary/target/capture probe/AuNPs/WS_2-MWCNTs/GCE (i). (F) Plot of Q-t curves of the bare GCE (a) and AuNPs/WS_2-AB/GCE (b) in 0.1 mM $K_3[Fe(CN)_6]$ containing 1.0 M KCl; (G) plot of

355 Q-$t^{1/2}$ curves on GCE (a) and AuNPs/WS_2-MWCNTs/GCE (b); (H) DPVs of
356 HRP/HCR/auxiliary/target/probe/BSA/AuNPs/GCE (a) and
357 HRP/HCR/auxiliary/target/probe/BSA/AuNPs/WS_2-AB/GCE (b) in 0.1 M PBS (7.0)
358 containing 1.8 mM H_2O_2 and 2 mM HQ.

359

360 EIS is one important tool for probing the features of surface-modified electrodes.
361 In the impedance spectra, the increase in the diameter of the semicircle indicates the
362 enhancement in the interfacial electron transfer resistance (R_{et}). When AB (curve b) or
363 WS_2-AB composites (curve c) are applied on the GCE, the R_{et} displays smaller value
364 than bare GCE (curve a) due to their good conductivity (Figure 3D). However, the R_{et}
365 of WS_2-AB composites show the lowest value, indicating the good conductivity of
366 WS_2-AB. When AuNPs are further electrodeposited on the WS_2-AB/GCE, the R_{et}
367 decreases obviously with an almost straight line (curve d), which is ascribed to the
368 excellent conductive ability of the AuNPs/WS_2-AB film. When the capture probe is
369 further immobilized on the electrode (curve e), the R_{et} value increases greatly because
370 the electrostatic repulsion between anionic $[Fe(CN)6]^{3-/4-}$ and the negatively charged
371 phosphate backbone (Figure 3E). After treated with BSA, the R_{et} value further
372 decreases (curve f). Following adding target DNA results in the R_{et} increasing
373 dramatically (curve g) due to the hybridization between target DNA and capture
374 probes. Similarly, the R_{et} increases when auxiliary DNA is applied on the electrode
375 surface (curve h). After HCR triggered by the recognition probe with bio-H1 and
376 bio-H2, the R_{et} increases significantly (curve i) due to more DNAs are immobilized on
377 the electrode surface, which make the electron transfer become more difficult. These
378 results indicated that the biosensor is effectively constructed.

The effective surface areas of GCE and AuNPs/WS_2-AB/GCE were compared by chronocoulumetry in 0.1 mM $K_3[Fe(CN)_6]$ solution containing 1.0 M KCl, where the standard diffusion coefficient (D_0) of $K_3[Fe(CN)_6]$ at 25 °C is 7.6×10^{-6} $cm^2\ s^{-1}$. The effective surface area (A) of electrodes is calculated according to the following equation:

$$Q = 2nFAcD^{1/2}t^{1/2}/\pi^{1/2} + Q_{dl} + Q_{ads} \quad (1)$$

where n is the number of electron transferred, F (C mol^{-1}) is the Faraday constant, A (cm^2) is the area of the electrode, c (mol cm^{-3}) is the concentration of substrate, D ($cm^2\ s^{-1}$) is the diffusion coefficient, Q_{dl} (C) is the double layer charge and Q_{ads} (C) is the adsorption charge and other symbols have their usual significances. According to the results shown in Figure 3F and 3G, A is calculated to be 0.072 cm^2 and 0.151 cm^2 for bare GCE and AuNPs/WS_2-AB/GCE, respectively. The results indicated that the effective surface area of the electrode increased greatly after modification with AuNPs/WS_2-AB film, which would increase the immobilization amount of the capture DNA and therefore improved the sensitivity of the sensor.

Figure 3H shows the signal-amplification effect of the as-prepared material. Current signal greatly increases when the WS_2-AB is employed in the sensor construction (curve b). The corresponding signal obtained in the presence of WS_2-AB composites (curve b) is about 214.3% for that in the absence of WS_2-AB composites (curve a), indicating the WS_2-AB composites are helpful to enhance detection sensitivity.

3.4. Optimization of experimental conditions

To obtain good analytical performance, several experimental conditions were optimized. The deposition time of AuNPs plays an important role in the size of the AuNPs. The effect of deposition time of AuNPs was tested in the range of 10–120 s (Figure 4 A). The peak current increases in the deposition time range of 10-60 because more and more AuNPs are formed on the electrode. The current response decreases after 60 s due to the formation of the big AuNPs, which reduces the active sites. So 60 s of deposition time was used.

The hybridization reaction temperature on the DPV response was investigated at different temperatures (20, 25, 30, 32, 35, 37, 40, 42, 45, 50 °C) (Figure 4 B). The results show that the DPV response increases along with the increase of the reaction temperature in the range of 20-37 °C, indicating the extension of the length of DNA duplex. The peak current then decreases from 37 to 50 °C because the higher temperature will destroy the DNA duplex construction. So 37 °C was chosen in all subsequent hybridization reaction.

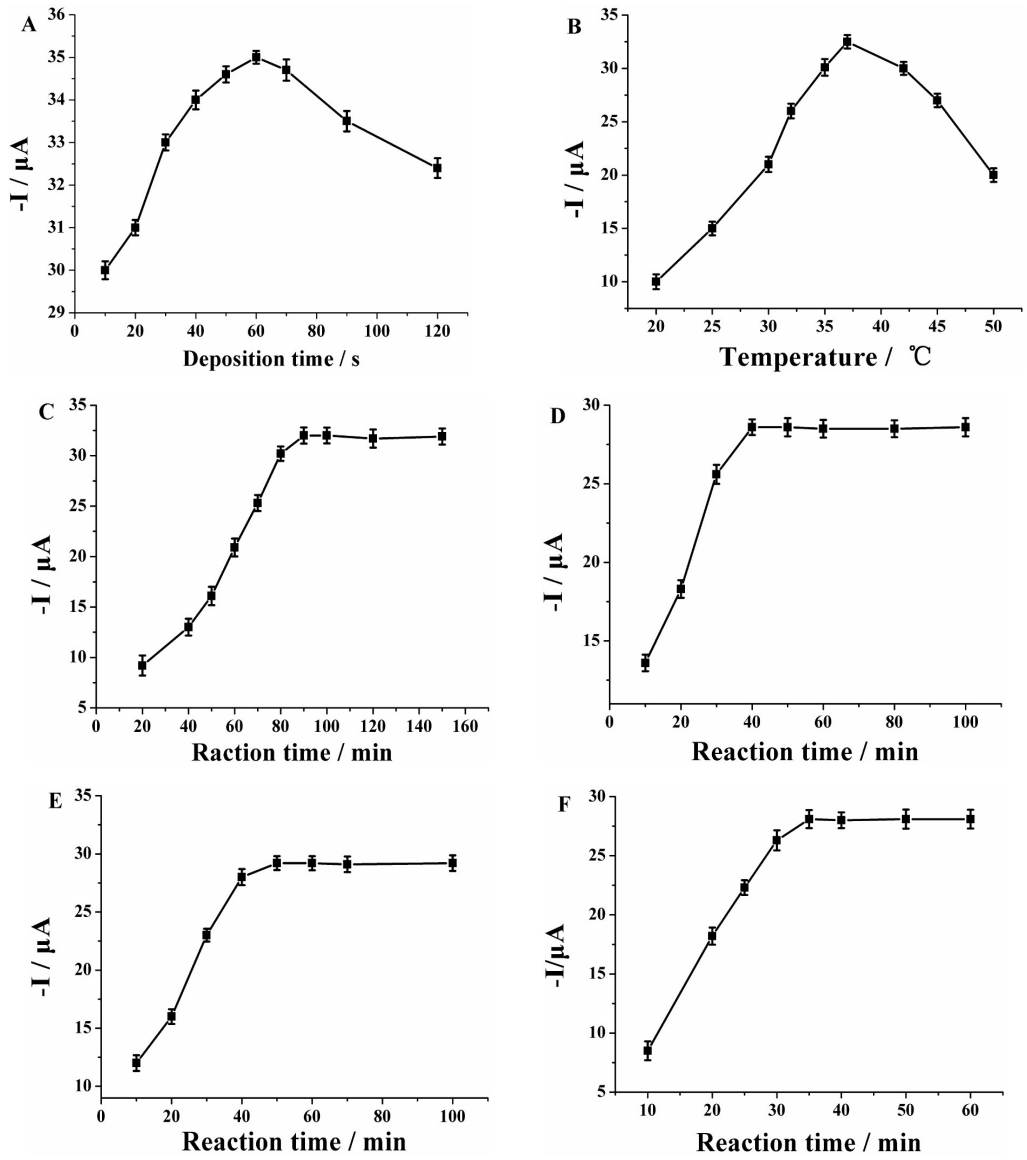

Figure 4. Effects of deposition time of AuNPs (A), hybridization temperature (B), the hybridization time between capture probe and target DNA (C), target DNA and auxiliary DNA (D), HCR (E) and self-assembly time of HRP (F) on the peak current.

The effect of the hybridization reaction time between capture probe and target DNA on the DPV response of $[Fe(CN)_6]^{-3/-4}$ was evaluated. As shown in Figure 4 C, the peak current increases rapidly when the reaction time ranges from 20 to 150 min, and almost stays stable after 90 min, suggesting the hybridization reaction is completed. Thus, 90 min of hybridization reaction time was used. Similarly, the

hybridization reaction time between target DNA and auxiliary DNA on the DPV response was also evaluated. As we can see from Figure 4 D, the DPV response intensifies with the reaction time increasing and keeps constant to a saturation value after 40 min, indicating that a 40 min reaction time is efficient for the hybridization of target DNA and auxiliary DNA.

The HCR time was studied in the range of 10-90 min (Figure 4 E). The result shows that the DPV response increases greatly in the HCR time range of 10-40 min, and then almost keeps stable when it exceeds 50 min. This result indicates that the HCR is primitively completed at 50 min. Therefore, 50 min was employed in the subsequent experiments.

Self-assembly time of HRP on the DPV response was also investigated. As shown in Figure 4 F, the DPV response increases gradually with the augment of reaction time and then tends to be constant after 35 min, which indicates the maximum HRP has been immobilized on the electrode. Thus, 35 min was used.

3.5. Optimization detection system

In this work, the detection system was based on HRP catalysis of the oxidation substrate of H_2O_2 + HQ. Herein, HQ plays as an electroactive mediator of shuttling electrons from the electrode surface to the redox center of HRP. Therefore, the catalytic reduction mechanism of H_2O_2 by the immobilized HRP can be described as follows: firstly, H_2O_2 substrate is reduced to H_2O by the immobilized HRP in reduced state (HRP_{Red}), and HRP_{Red} itself will turn into its oxidized state HRP_{Ox}. Then, HQ

can reverse HRP_{Ox} back into HRP_{Red} and be oxidized into benzoquinone (BQ). BQ can engage in electron exchange with the electrode and itself turns back into HQ. Therefore, HQ recycles in the system causing the amplification of the reduction current. The reaction mechanism of the catalytic process can be expressed as follows:[32]

$$H_2O_2 + HRP_{Red} \rightarrow HRP_{Ox} + H_2O \quad (2)$$

$$HRP_{Ox} + HQ \rightarrow BQ + HRP_{Red} \quad (3)$$

$$BQ + 2H^+ + 2e \rightarrow HQ \quad (4)$$

The pH of solution and the concentration of the substrate are the important factors influencing the detection sensitivity due to pH can affect the biological activity of HRP. The effect of pH was tested in the range of 4-9. The highest DPV response is obtained at pH 7 (Figure 5 A). The effect of H_2O_2 concentration was also studied. As shown in Figure 5 B, the DPV response increases with the increase of H_2O_2 concentration in the range of 0-3.4 mM, and then almost stays stable when it exceeds 1.8 mM. Similarly, the effect of HQ concentration was evaluated in the range of 0-3.5 mM. As shown in Figure 5C, the current response increases with the increase of HQ concentration in the range of 0-2.0 mM, and then almost keeps stable when it exceeds 2 mM. Thus, 2 mM HQ and 1.8 mM H_2O_2 were selected.

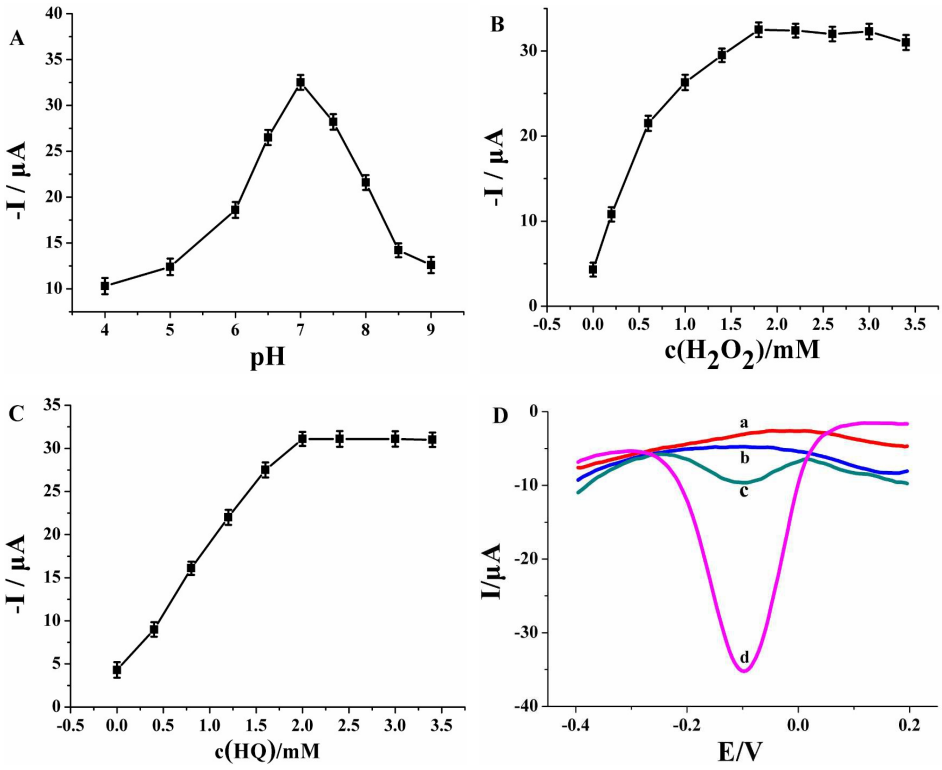

Figure 5. (A) The current response of the biosensor in PBS containing and 1.8 mM H_2O_2 and 2 mM HQ at different pH values. (B) The current response of the biosensor in PBS (pH 7.0) containing different H_2O_2 concentrations. (C) The current response of the biosensor in PBS (pH 7.0) containing different HQ concentrations. (D) DPVs of HRP/HCR/auxiliary/target/probe/BSA/AuNPs/WS_2-AB/GCE electrode in 0.1 M PBS (7.0) containing 0 (a), 1.8 mM H_2O_2 (b), 2 mM HQ (c) and 1.8 mM H_2O_2 + 2 mM HQ (d). Error bars represent the standard deviation of three repeat measurements

The electrocatalytic activity of the HRP on the electrode toward HQ+H_2O_2 was studied. As seen in Figure 5D, no redox response is observed in pH 7.0 PBS without H_2O_2 and HQ (curve a) or only with H_2O_2 (curve b). A low reduction peak is obtained when 2.0 mM HQ is added (curve c). Then, when 1.8 mM H_2O_2 + 2.0 mM HQ is added, a significant reduction peak is observed (curve d). On the basis of these results, we might reach a conclusion that the HRP electrode coupled with HQ + H_2O_2 system could amplify the detection signal.

3.6. The signal amplification effect of HCR

Herein, a single auxiliary DNA can induce a chain of H1-H2 probes to be hybridized and captured on the electrode surface. H1-H2 probes are labeled by biotin, so they allow further capture of a lot of HRP. HRP can catalyze the inactive HQ to an electrochemically active BQ, which can be detected using DPV. In order to validate the signal amplification effect of HCR, the electrochemical performances of different electrodes were compared. As shown in Figure 6, the electrode modified with the mixture of bio-H1 and bio-H2 (curve a) shows a much more remarkable signal than the electrode only modified with bio-H1 (curve b), bio-H2 (curve c) and the blank (curve d), which demonstrates HCR can greatly improve the sensitivity of the sensor.

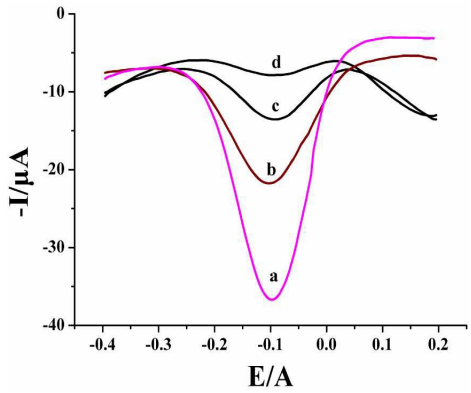

Figure 6. DPV curves responding to 1 pM target DNA immersed in the mixture of bio-H1 and bio-H2 (a), only immersed in bio-H1 (b), only immersed in bio-H2 (c), and immersed in blank (d).

3.7. Analytical performance of designed biosensor

Under the optimal conditions, various concentrations of target DNA were detected. Figure 7 shows the peak current increases with the increasing concentration of target DNA. There was a good linear relationship between the peak current and the

logarithm of the target DNA concentration in the range of 0.001-100 pM. The linear calibration equation was i(μA) = -5.08 log(c/M) - 85.43 (i is the peak current and c is the concentration of target DNA) with a correlation coefficient (R) of 0.997. The detection limit was calculated to be 1.2×10^{-16} M based on three times the standard deviation of the blank sample measurement. The analytical performances of different assays are compared in Table 3. The proposed assay exhibits the lowest detection limit and the widest detection range.

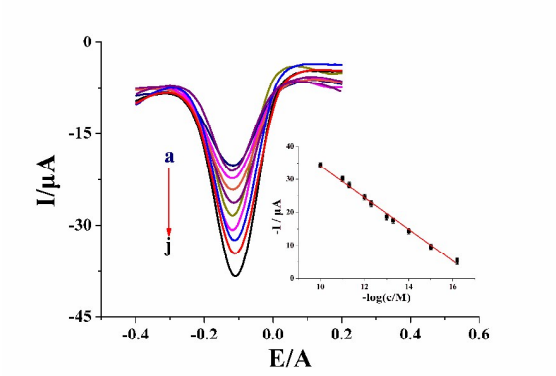

Figure 7. DPV curves responding to different target DNA concentrations (from a to j): 0, 1.0×10^{-15}, 1.0×10^{-14}, 5.0×10^{-14}, 1.0×10^{-13}, 5.0×10^{-13}, 1.0×10^{-12}, 5.0×10^{-12}, 1.0×10^{-11}, 1.0×10^{-10} M, respectively. Inset: the relationship between the peak current and the negative logarithm of the target DNA concentration.

532 **Table 3** Comparison between the proposed assay and other reported method for DNA
533 detection.

Electrodes	Analytical technique	Linear range (nM)	LOD (pM)	References
Phenylenediamine-NH_2/GO/GCE	EIS	0.001–100	0.11	33
Gr-AuNPs/GCE	Amperometric current–time curve	0.00005–100	0.0034	34
Gr/polyaniline/GCE	DPV	0.0001–700	0.032	35
CeO_2–single-walled carbon nanotubes–1-butyl-3-methylimidazolium hexafluorophosphate/GCE	EIS	0.001–100	0.23	36
Chit–CeO_2–ZrO_2/Au	DPV	0.000163–16.3	0.1	37
CeO_2/Chit/GCE	DPV	0.0159–116	10	38
4-aminothiophenol/AuNPs/Au	DPV	0.014–2	9.5	39
WS_2-Gr/GCE	DPV	0.00001–0.5	0.0023	40
AuNPs/WS_2-AB/GCE	DPV	0.000001–0.1	0.000115	This work

534

535 **3.8. Specificity, repeatability and stability**

536 In order to validate the selectivity of the developed biosensor, different DNA
537 sequences including noncomplementary sequence, three-based mismatch sequence,
538 one-based mismatch sequence and the complementary sequence were tested with the
539 developed biosensor. As shown in Figure 8, the higher peak current is observed when
540 the complementary sequence is used, indicating good specificity of the proposed
541 biosensor.

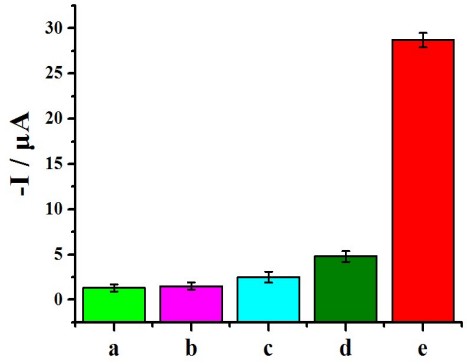

Figure 8. The specificity of the HCR-based DNA sensor hybridized to different target sequences: blank (PBS 7.0) (a), 1.0×10^{-11} M noncomplementary sequence (b), 1.0×10^{-11} M three-based mismatch sequence (c), 1.0×10^{-11} M one-based mismatch sequence (d) and 1.0×10^{-11} M complementary sequence (e).

The reproducibility of the developed biosensor was estimated. The peak currents of ten successive measurements of 1×10^{-14} M target DNA by DPV were determined and a relative standard deviation (RSD) of 2.1% was obtained. Eight parallel-made biosensors were used to detect 1×10^{-14} M target DNA and a RSD of 3.8% was achieved, indicating good reproducibility. The stability of proposed biosensor was also investigated. When the biosensor was stored at 4 °C for 15 days, it retained 94.6% of its initial current response, indicating good stability.

3.9. Serum samples analysis

In order to verify the general applicability of proposed assay for real-sample analysis, the developed biosensor was used to detect the target DNA in serum samples. The serum sample was diluted to 1:10 with PBS (pH 7.0). 0.1 M PBS (pH 7.0) and the serum sample were then spiked with three target DNA concentrations (0.01 pM, 5 pM, 100 pM), respectively. The samples were then detected with the proposed assay. The

peak currents of three spiked target DNA concentrations were close in serum (13.6, 20.9, 33.2 μA) and in 0.1 M PBS (14.3, 22.6, and 34.3 μA), which indicated good potential of the developed assay for clinical applications.

4. Conclusions

In summary, an ultrasensitive electrochemical DNA biosensor was developed for detection of target DNA based on HCR integrating a novel WS_2-AB composite. The WS_2-AB composites possessed large specific surface area and good biocompatibility, which not only increased the immobilization amount of AuNPs and efficiently accelerated the electron transfer, but also retained the active immobilized biomolecules and enhanced the stability of the DNA probe. The proposed DNA sensor showed low detection limit (0.12 fM), wide linear range (0.001 M to 100 pM) and satisfactory selectivity. Compared with traditional methods for target DNA, major advantages of the propose assay are high sensitivity, wide response linearity and rapid readout of target DNA, and it has a great potential for versatile applications in genetic target analysis in bioanalytical, clinic diagnostics and mutation identification.

Acknowledgments

This work was supported by the National Natural Science Foundation of China (U1304214, 21475115) and Program for University Innovative Research Team of Henan (15IRTSTHN001), Henan Provincial Science and technology innovation team (C20150026), Nanhu Scholars Program of XYNU and Graduate Students

584 Sustentation Fund of Xinyang Normal University (No. 2015KYJJ34).

585

586 References

587 1 X.L, Zhu, L.Y. Sun, Y.Y. Chen, Z.H. Ye, Z.M. Shen and G.X. Li, Biosens.
588 Bioelectron. 2013, **47**, 32.
589 2 D.F Luo, X. Liu, L.L. Wang and Z.Z. Ma, J. Xinyang Normal Univ. (Nat. Sci. Ed.)
590 2014, **27**, 538.
591 3 Z.Y. Peng, B. Young, A.E. Baird and S.A. Soper, Anal. Chem. 2013, **85**, 7851.
592 4 Z.Y. Peng, S.A. Soper, M.R. Pingle, F. Barany and L.M. Davis, Anal. Chem. 2010,
593 **82**, 9727.
594 5 J.M. Emory, Z.Y. Peng, B. Young, M.L. Hupert, A. Rousselet, D. Patterson, B.
595 Ellisond and S.A. Soper, Analyst, 2012, **137**, 87.
596 6 Z.Y. Peng, J. Shihezi Univ. (Nat. Sci.) 2014, **32**, 371.
597 7 J.M. Emory, Z.Y. Peng, F. Crawford-Drake, P.C. Chen, M.C. Murphy and S.A.
598 Soper, Twelfth International Conference on Miniaturized Systems for Chemistry and
599 Life Sciences, San Diego, California, USA 2008, 402.
600 8 Z.Y. Peng, Signle-molecule detection of molecular beacons generated from LDR on
601 thermoplastic microfluidic device for bioanalysis (Doctor Thesis), Louisiana State
602 University, Baton Rouge, Louisiana, United States, 2012.
603 9 Y. Wan, H. Xu, Y. Su, X.H. Zhu, S.P. Song and C.H. Fan, Biosens. Bioelectron.
604 2013, **41**, 526.
605 10 W. Ren, Z.F. Gao, N.B. Li and H.Q. Luo, Biosens. Bioelectron. 2015, **63** 153.

606 11 K.J. Huang, Y.J. Liu, H.B. Wang, Y.Y. Wang and Y.M. Liu, Biosens. Bioelectron.
607 2014, **55**, 195.
608 12 Y. Qian, C.Y. Wang and F.L. Gao, Biosens. Bioelectron. 2015, **63**, 425.
609 13 S.F. Liu, Y. Wang, J.J. Ming, Y. Lin, C.B. Cheng and F. Li, Biosens. Bioelectron.
610 2013, **49**, 472.
611 14 B.P. Ting, J. Zhang, Z.Q. Gao and J.Y. Ying, Biosens. Bioelectron. 2009, **25**, 282.
612 15 G. Liu, Y. Wan, V. Gau, J. Zhang, L. Wang and S. Song, C. Fan, J. Am. Chem.
613 Soc. 2008, **130**, 6820.
614 16 H. Li, Z. Sun, W. Zhong, N. Hao, D. Xu and H.Y. Chen, Anal. Chem. 2010, **82**,
615 5477.
616 17 Y. Jin, X. Yao, Q. Liu and J. Li, Biosens. Bioelectron. 2007, **22**, 1126.
617 18 J. Zhao, S.S. Hu, Y. Cao, B. Zhang and G.X. Li, Biosens. Bioelectron. 2015, **66**,
618 327.
619 19 Z.L. Ge, M.H. Lin, P. Wang, H. Pei, J. Yan, J.Y. Shi, Q. Huang, D.N. He, C.H.
620 Fan and X.L. Zuo, Anal. Chem. 2014, **86**, 2124.
621 20 X.Z. Hu, P. Wang, J.Q. Yang, B. Zhang, J. Li, J. Luo and K.B. Wu, Colloids Surf.
622 B 2010, **81**, 27.
623 21 Y.Y. Zhang, Y.Y. Wang, K.B. Wu, S.C. Zhang, Y. Zhang and C.D. Wan, Colloids
624 Surf. B 2013, **103**, 94.
625 22 K.J. Huang, Y.J. Liu, J.Z. Zhang, J.T. Cao and Y.M. Liu, Biosens. Bioelectron.
626 2015, **67**, 184.
627 23 M. Pumera and A.H. Loo, Trends Anal. Chem. 2014, **61**, 49.
628 24 K.J. Huang, L. Wang, Y.J. Liu, H.B. Wang, Y.M. Liu and L.L. Wang, Electrochim.
629 Acta. 2013, **109**, 587.
630 25 D.F Luo and X. Liu, J. Xinyang Normal Univ. (Nat. Sci. Ed.) 2015, **28**, 542.

631 26 J. Li, Z.j. Yang, Y. Tang, Y.C. Zhang and X.Y. Hu, Biosens. Bioelectron. 2013, **41**,
632 698.
633 27 H.B. Wang, H.D. Zhang, Z.H. Xing, X.L. Li and Y. Chen, J. Xinyang Normal Univ.
634 (Nat. Sci. Ed.) 2015, **28**, 550.
635 28 H. Liu, D. Su, G. Wang and S.Z. Qiao, J. Mater. Chem. 2012, **22**, 17437.
636 29 C.B. Zhu, P. Kopold, W.H. Li, P.A.V. Aken, J. Maier and Y. Yu, J. Mater. Chem. A
637 2015, **3**, 20487.
638 30 R. Bhandavat, L. David and G. Singh, J. Phys. Chem. Lett. 2012, **3**, 1523.
639 31 Y. Yong, L. Zhou, Z. Gu, L. Yan, G. Tian, X. Zheng, X. Liu, X. Zhang, J. Shi, W.
640 Cong, W. Yin and Y. Zhao, Nanoscale, 2014, **6**, 10394.
641 32 S. Yang, W.Z. Jia, Q.Y. Qian, Y.G. Zhou and X.H. Xia, Anal. Chem. 2009, **81**,
642 3478.
643 33 Y.W. Hu, F.H. Li, D.X. Han, T.S. Wu, Q.X. Zhang, L. Niu and Y. Bao, Anal.
644 Chim. Acta 2012, **753**, 82.
645 34 K.J. Huang, J. Li, Y.Y. Wu and Y.M. Liu, Bioelectrochemistry 2013, **90**, 18.
646 35 A.L. Liu, G.X. Zhong, J.Y. Chen, S.H. Weng, H.N. Huang, W. Chen, L.Q. Lin, Y.
647 Lei, F.H. Fu, Z.L. Sun, X.H. Lin, J.H. Lin and S.Y. Yang, Anal. Chim. Acta 2013,
648 **767**, 50.
649 36 M. Du, T. Yang, X. Li and K. Jiao, Talanta 2012, **88**, 439.
650 37 W. Zhang, T. Yang, X. Zhuang, Z. Guo and K. Jiao, Biosens. Bioelectron. 2009,
651 **24**, 2417.
652 38 Q.X. Wang, F. Gao, X. Zhang, B. Zhang, S.X. Li, Z.S. Hu and F. Gao,
653 Electrochim. Acta 2012, **62**, 250.
654 39 K.J. Feng, Y.H. Yang, Z.J. Wang, J.H. Jiang, G.L. Shen and R.Q. Yu, Talanta
655 2006, **70**, 561.

656 40 K.J. Huang, Y.J. Liu, H.B. Wang, T. Gan, Y.M. Liu and L.L. Wang, Sensor.
657 Actuat. B 2014, **191**, 828.

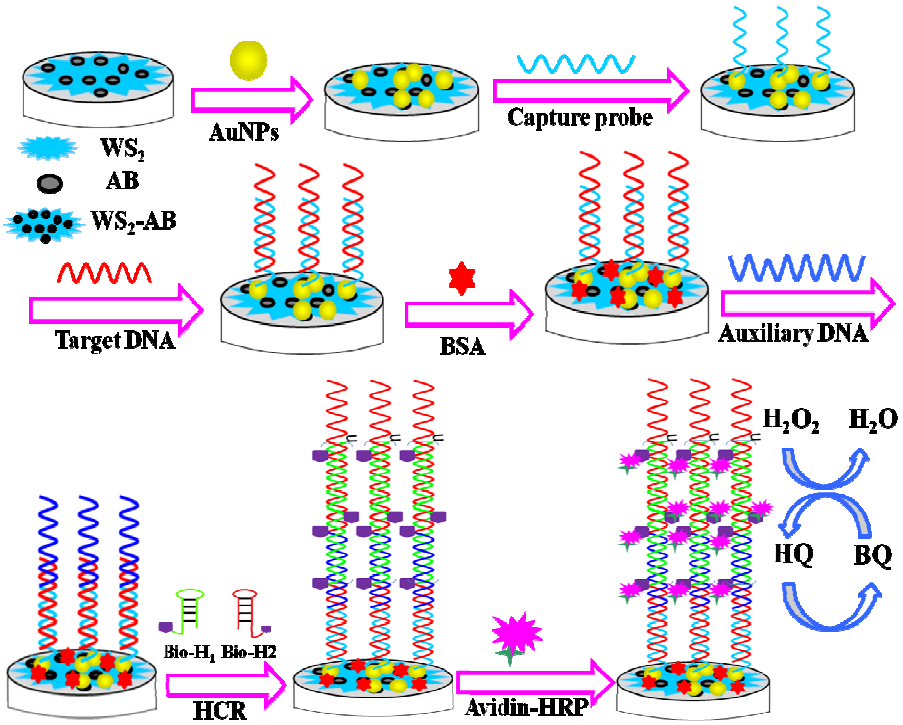

An electrochemical biosensor is constructed to sensitively detect DNA sequences based on tungsten disulfide/acetylene black composites and hybridization chain reaction.